Supplementary Information

A Highly Efficient Electrolysis System Enabled by Direct Impedance Matching Between Charge Migration Triboelectric Nanogenerator and Series Connected Electrolysers

Yu Deng[a], Qian Qin[a], Wencong He[a], Hengyu Guo[b], Jie Chen[a,*]

[a] *College of Physics and Electronic Engineering, Chongqing Normal University, Chongqing 401331, China*

[b] *School of Physics, Chongqing University, Chongqing, 400044, China*

Correspondence to: chenjie@cqnu.edu.cn (J. Chen)

Keywords: Triboelectric nanogenerator, Charge migration, Direct impedance matching, Series-connected electrolysers, Seawater electrolysis

Content

Supplementary Note

Supplementary Figures

Fig. S20 Physical photographs of hydrogen production for different electrode materials in 12.5 wt% saline solution.

Fig. S21 Chronopotentiometry testing of Ti@Pt in simulated seawater with 12.5 wt% salinity at a constant current density of 3.5 mA cm^{-2} for 10 hours.

Fig. S22 a)-b) Structure diagram of sliding CM-TENG and the peak power under different external resistances.

Fig. S23 a) Dependence of CM-TENG's output current on number of SCEs. b) Output energy per unit time of CM-TENG when connected with 200 SCEs.

Fig. S24 Generation of O_2 and H_2 per minute.

Fig. S25 a)-d) Physical photographs of Unit 1's stator, and Unit 2's stator, the deposited grid-shaped copper electrodes, and the rotor.

Fig. S26 Physical photograph of CM-TENG' overall structure.

Supplementary Movies

Movie S1. H_2 generated by motor-driven CM-TENG with 200 SCEs.

Movie S2. H_2 generated by CM-TENG with PMC.

Movie S3. H_2 generated by wind-driven CM-TENG with 200 SCEs.

Note. S1 Analysis of the powered-managed CM-TENG.

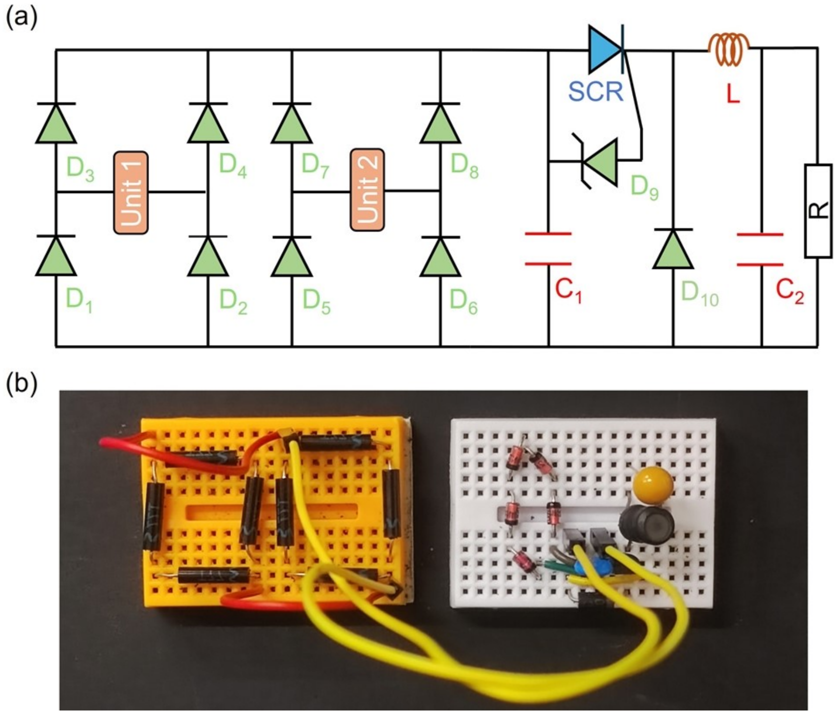

Fig. N1 a)-b) Circuit diagram and physical photograph of the powered-managed CM-TENG.

The circuit of the powered-managed CM-TENG is divided into two parts, as shown in Fig. N1. The first part is the rectifier section, which utilizes eight diodes (D_1-D_8) to form two rectifier bridges, allowing Unit 1 and Unit 2 to be rectified and effectively eliminating phase effects. After rectification, the two units are connected in parallel and linked to the PMC (Unit 1//Unit 2 with PMC). The components of the PMC include a high voltage ceramic capacitor (C_1: 2 kV, 681 pF), a silicon-controlled rectifier (SCR), a zener diode (D_9), a diode (D_{10}), an inductor (L), and a tantalum capacitor (C_2: 25 V, 100 μF). Initially, the current of Unit 1//Unit 2 flows into C_1, causing its voltage to gradually increase. Once the voltage of C_1 exceeds the reverse voltage of D_9 and maximum working voltage of C_2, D_9 enters reverse conduction. This action triggers the SCR to open, allowing energy to be transferred from C_1 to L, C_2, and R. As the voltage across C_1 decreases to zero, D_{10} commences forward conduction, stabilizing the voltage across C_1 around zero and keeping both the current through C_1 and SCR at zero. This process effectively reduces the output voltage of the CM-TENG while increasing the current, resulting in a reduced matching impedance of 20 kΩ (Fig. N2). However, the PMC inevitably introduces energy losses, resulting in the energy utilization efficiency of the power-managed CM-TENG:

$$\eta_1 = \frac{(\bar{P}_{Unit\ 1//Unit\ 2\ with\ PMC})max}{(\bar{P}_{Unit\ 1//Unit\ 2})max} \times 100\% = 55.4\% \tag{N1}$$

While the energy utilization efficiency of the direct rectified CM-TENG is given by

$$\eta_2 = \frac{(\bar{P}_{Unit\ 1//Unit\ 2})max}{(\bar{P}_{Unit\ 1})max + (\bar{P}_{Unit\ 2})max} \times 100\% = 99.0\% \tag{N2}$$

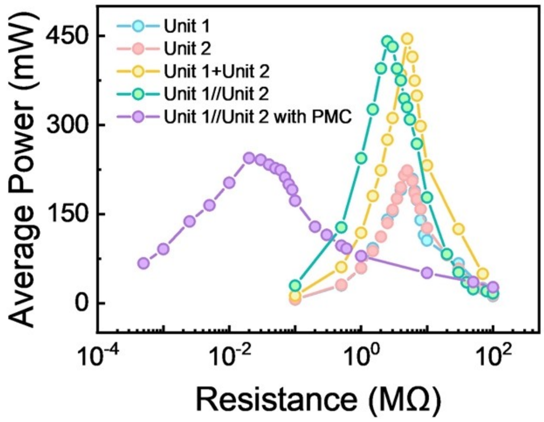

Fig. N2 Average power of Unit 1, Unit 2, Unit 1+Unit 2, Unit 1//Unit 2, and Unit 1//Unit 2 with PMC under different external resistances.

Note. S2 Factors influencing the impedance of CM-TENG.

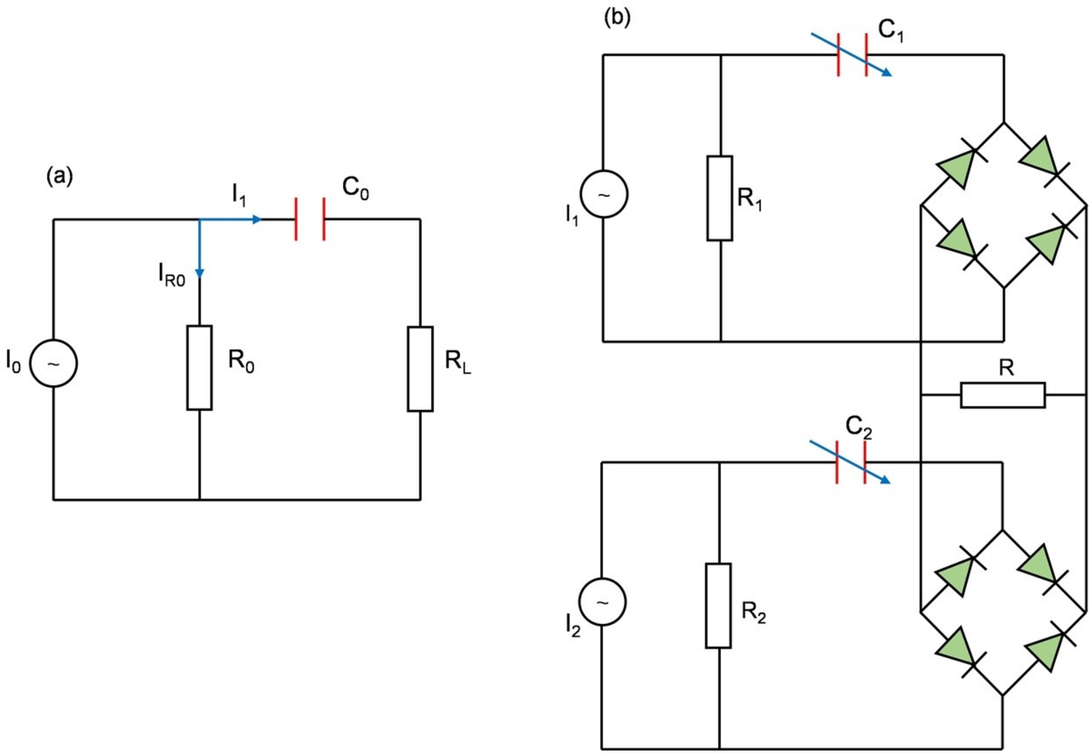

Fig. N3 a)-b) Equivalent circuit model of TENG and double-layer parallel connection CM-TENG.

The equivalent circuit model of TENG is established from Kirchoff's current law at the junctions, as shown in Fig. N3. I_l represents the equivalent current of TENG, R_0 denotes its internal resistance, C_0 indicates its internal capacitance, and R_l is the external load resistance. That is, the internal current I_0 is the sum of the current of the internal resistor I_{R_0} and the current I_l in the outer branch connected the load:

$$I_0 = I_l + I_{R_0} \tag{N3}$$

The relationship between these currents is given by:

$$\frac{I_{R_0}}{I_l} = \frac{\sqrt{\left(\frac{1}{2\pi f C_0}\right)^2 + R_l^2}}{R_0} \tag{N4}$$

Thus, the output power of TENG can be expressed as:

$$P = I_l^2 R_l = \left(\frac{I_0 R_0}{R_0 + \sqrt{\left(\frac{1}{2\pi f C_0}\right)^2 + R_l^2}} \right)^2 R_l \tag{N5}$$

When the external load matches the impendence of TENG (z_0), P reaches its maximum value. To find this condition, we set the derivative to zero:

$$\frac{\partial P}{\partial R_l} = 0 \Longrightarrow \frac{I_0^2 R_0^2}{\left(R_0 + \sqrt{\left(\frac{1}{2\pi f C_0}\right)^2 + R_l^2}\right)^2} - \frac{2 I_0^2 R_0^2 R_l^2}{\left(R_0 + \sqrt{\left(\frac{1}{2\pi f C_0}\right)^2 + R_l^2}\right)^3 \sqrt{\left(\frac{1}{2\pi f C_0}\right)^2 + R_l^2}} = 0 \tag{N6}$$

This simplifies to:

$$\left(R_0 + \sqrt{\left(\frac{1}{2\pi f C_0}\right)^2 + R_l^2}\right)\sqrt{\left(\frac{1}{2\pi f C_0}\right)^2 + R_l^2} - 2R_l^2 = 0 \tag{N7}$$

Let $x = \sqrt{\left(\frac{1}{2\pi f C_0}\right)^2 + R_l^2}$, Equation N7 becomes

$$(R_0 + x)x - 2\left(x^2 - \left(\frac{1}{2\pi f C_0}\right)^2\right) = 0 \tag{N8}$$

The solution for x are：

$$x = \frac{R_0 \pm \sqrt{R_0^2 + 8\left(\frac{1}{2\pi f C_0}\right)^2}}{2} \tag{N9}$$

Only the positive solution is considered. Substituting the result back into the expression for x:

$$\left(\frac{1}{2\pi f C_0}\right)^2 + R_l^2 = \left(\frac{R_0 + \sqrt{R_0^2 + 8\left(\frac{1}{2\pi f C_0}\right)^2}}{2}\right)^2 \tag{N10}$$

Through simplification

$$R_l = \sqrt{\frac{R_0^2 + R_0\sqrt{R_0^2 + 8\left(\frac{1}{2\pi f C_0}\right)^2} + 2\left(\frac{1}{2\pi f C_0}\right)^2}{2}} = z_0 \tag{N11}$$

For the double-layer parallel connection CM-TENG, let I_1, R_1 and C_1 represent the current, internal resistance, and internal capacitance of Unit 1, while I_2, R_2 and C_2 correspond to Unit 2. The external load resistance is denoted as R. Ignoring the effects of the rectifier bridge, the total impedance of the CM-TENG (z) is given by:

$$z = \frac{z_1 z_2}{z_1 + z_2} \tag{N12}$$

where z_1 and z_2 are the impedance of Unit 1 and Unit 2, respectively. When Unit 1 and Unit 2 are identical and operate under the same conditions, $z_1 = z_2$, allowing for simplification:

$$z = \frac{z_1}{2} = \frac{1}{2}\sqrt{\frac{R_1^2 + R_1\sqrt{R_1^2 + 8\left(\frac{1}{2\pi f C_1}\right)^2} + 2\left(\frac{1}{2\pi f C_1}\right)^2}{2}} \tag{N13}$$

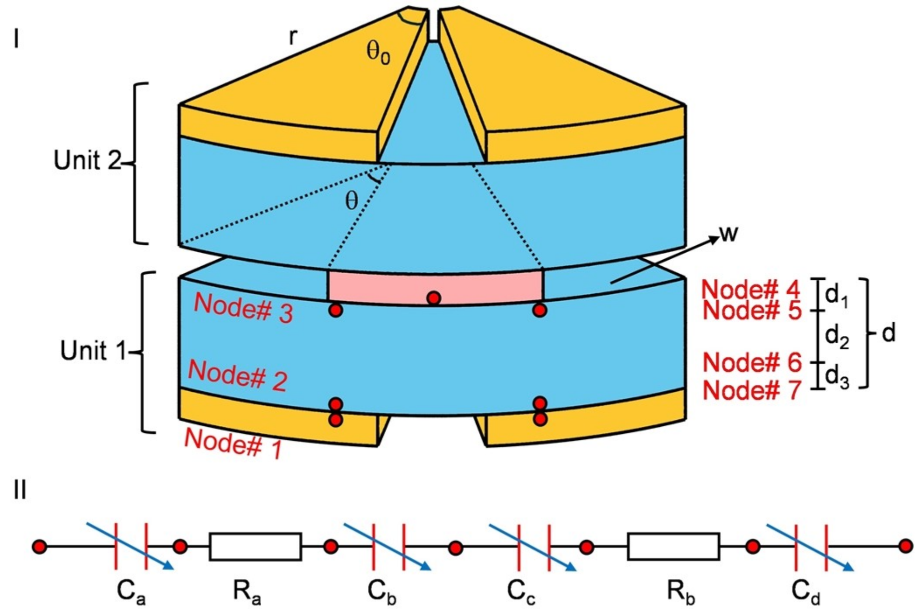

Fig. N4 Equivalent nodes circuit of CM-TENG.

In Fig. N4, the nodal method is used to analyze the intrinsic resistance and capacitance of CM-TENG. Taking a set of electrodes from Unit 1 as an example, the equivalent capacitance (C_1) is determined by:

$$\frac{1}{C_1} = \frac{\theta_0}{\pi}\left(\frac{1}{C_a} + \frac{1}{C_d} + \frac{1}{C_b} + \frac{1}{C_c}\right) \tag{N14}$$

where θ_0 represents the electrode degree. By virtue of symmetry, Capacitance between #1 and #2 (C_a), #6 and #7 (C_d) are equivalent. However, affected by charge migration within the PU, these capacitances are reformulated as:

$$C_a = \frac{\varepsilon_r s_0}{4\pi k d_3} \tag{N15}$$

$$C_d = \frac{\varepsilon_r s_0}{4\pi k d_3^{'}} \tag{N16}$$

$$s_0 = \frac{1}{2}\theta_0 r^2 \tag{N17}$$

where s_0, r, and k are the electrode area, electrode radius, and electrostatic force constant. d_3 and ε_r denote the dielectric layer thickness and its relative dielectric constant, respectively. The superscript on the dielectric layer thickness indicates changes in effective thickness due to charge migration. During the movement of PTFE, two variable capacities C_b and C_c are formed between nodes #3 and #4, #4 and #5.

$$C_b = \frac{\varepsilon_r s_1}{4\pi k d_1} \tag{N18}$$

$$C_c = \frac{\varepsilon_r s_2}{4\pi k d_1^{'}} \tag{N19}$$

$$s_1 = \frac{1}{2}(\theta_0 - \theta) r^2 \tag{N20}$$

$$s_2 = \frac{1}{2}\theta r^2 \tag{N21}$$

where s_1 and s_2 represent the contact area of left and right PTFE, while d_1 and θ correspond to the dielectric layer thickness and PTFE rotation angle, respectively. Substituting Equation N15-N21 into Equation N14 results in:

$$\frac{1}{2\pi f C_1} = \frac{2k}{\pi v}\left(\frac{2\theta_0\left(d_3 + d_3^{'}\right)}{\varepsilon_{r1} r^2} + \frac{2 d_1 \theta_0^{\,2}}{\varepsilon_{r2}\left(\theta_0 - \theta\right) r^2} + \frac{2\theta_0^{\,2} d_1^{'}}{\varepsilon_{r2}\theta r^2}\right) \tag{N22}$$

The equivalent resistance (R_1) can be expressed as:

$$R_1 = \frac{\theta_0}{\pi}(R_a + R_b) \tag{N23}$$

$$R_a = \rho \frac{d_2}{s_0} \tag{N24}$$

$$R_b = \rho \frac{d_2^{'}}{s_0} \tag{N25}$$

where R_a and R_b are the resistance between nodes #2 and #3, #5 and #6. The relevant resistivity and thickness are denoted by ρ, d_2 and $d_2^{'}$. Substituting Equation N17, N24, and N25 into N23 yields:

$$R_1 = \frac{2\rho\left(d_2 + d_2^{'}\right)}{\pi r^2} \tag{N26}$$

Moreover, the relationships among the working frequency f, rotational speed v, and total thickness d are given by:

$$f = \frac{\pi v}{\theta_0} \tag{N27}$$

$$d = d_1 + d_2 + d_3 \tag{N28}$$

Combining the qualitative analyses from Equation N13, N22, and N26 reveals that z is directly proportional to d and θ_0, while being inversely proportional to r and v. This relationship is consistent with the experimental results illustrated in Fig. 2.

Note. S3 Factors influencing the output power of CM-TENG.

The output power of the CM-TENG is qualitatively analyzed in terms of output voltage and current using Gauss's theorem and the current continuity equation. The potential difference between the two electrode pairs from the initial state to the final state can be obtained:

$$V_1 = \left(\frac{2d\sigma}{\varepsilon_0\varepsilon_r} - \frac{(-2)d\sigma}{\varepsilon_0\varepsilon_r}\right) \tag{N29}$$

where σ is the tribo-charge density of PU and ε_0 is the dielectric constant of vacuum. When the parallel connection units are identical, the equivalent voltage of multiple units remains consistent. Thus, the total voltage of CM-TENG is:

$$V = V_1 = \frac{4d\sigma}{\varepsilon_0\varepsilon_r} \tag{N30}$$

The transferred charge in one cycle can be expressed as:

$$Q = \frac{\theta_0}{\pi} \cdot \sigma \cdot \pi r^2 = \theta_0 \cdot \sigma r^2 \tag{N31}$$

Therefore, the output current of CM-TEMG (I_l) is determined by:

$$I = 2I_l = 2\frac{\pi}{\theta_0}Q \cdot f = 2\sigma\pi^2 \cdot \frac{r^2 v}{\theta_0} \tag{N32}$$

where I_l output current of Unit 1. Substituting I and V into power equation $P = IV$ yields:

$$P = IV = \frac{8\pi^2 d\sigma^2 r^2 v}{\varepsilon_0\varepsilon_r\theta_0} \tag{N33}$$

It is evident that output power is directly proportional to σ^2, r^2 and v, while inversely proportional to θ_0. However, an increase in thickness results in a reduction of the induced charge density. This phenomenon elucidates why a decrease in d from 3 mm to 1 mm can yield an enhancement in P (Fig. 2g-2j).

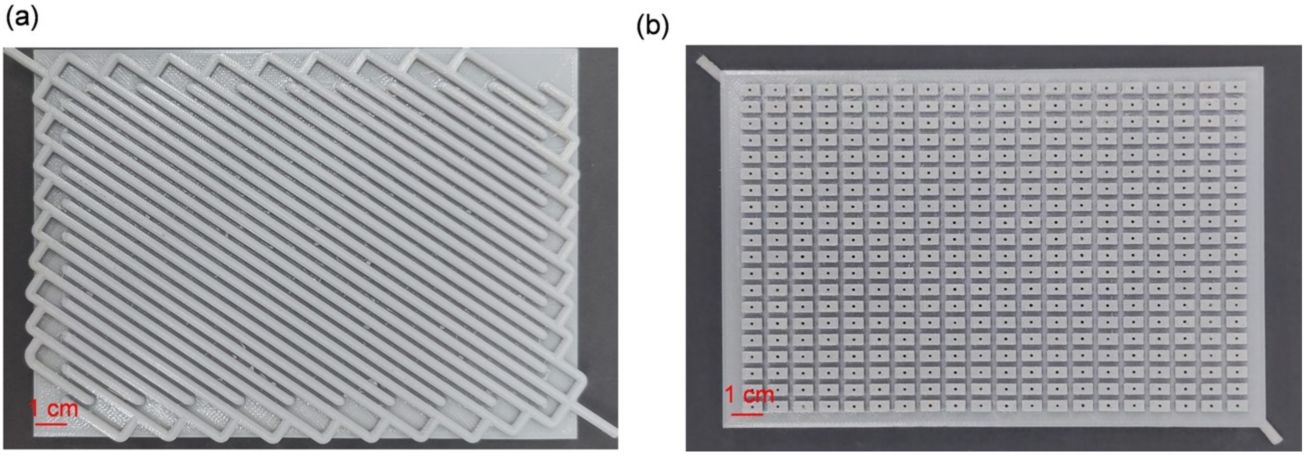

Fig. S1 a)-b) Physical photograph of collecting duct and collecting hole of cover.

(a) (b)

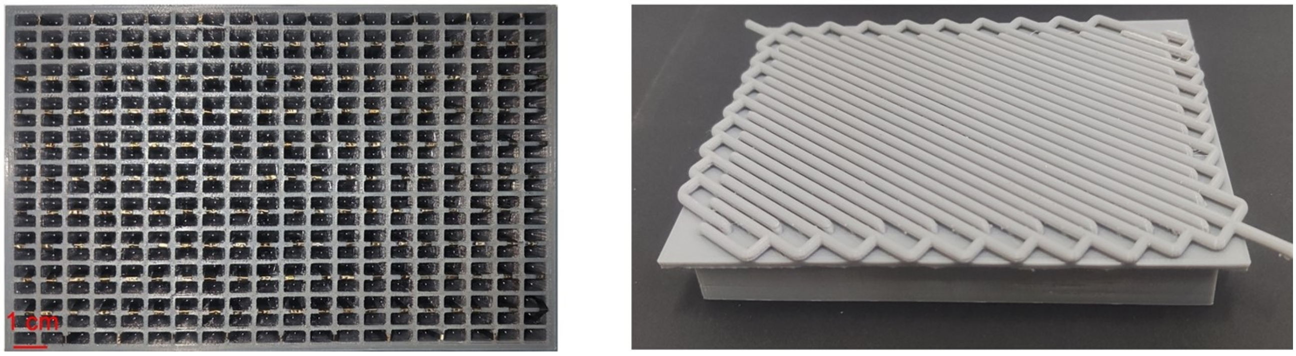

Fig. S2 a)-b) Physical photograph of the body and overall structure of SCEs.

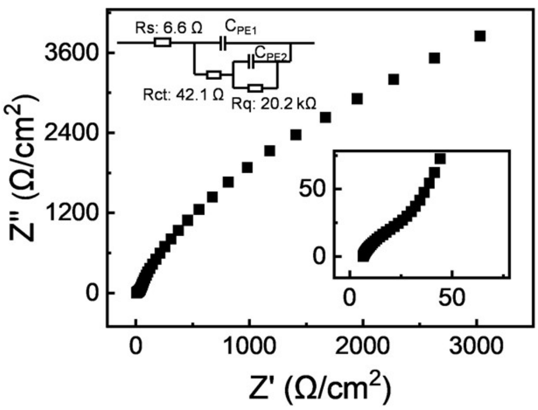

Fig. S3 EIS spectrum of a typical electrolyser.

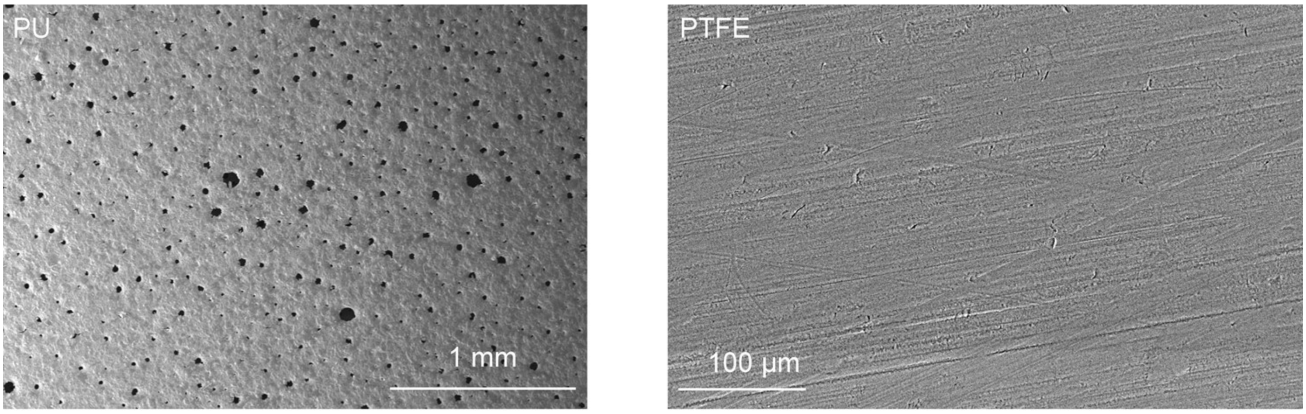

Fig. S4 Surface morphology of PU foam and PTFE.

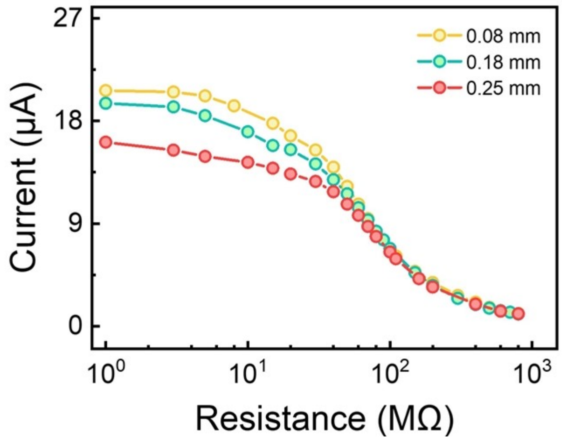

Fig. S5 Dependence of conventional TENG's output current on PTFE thickness.

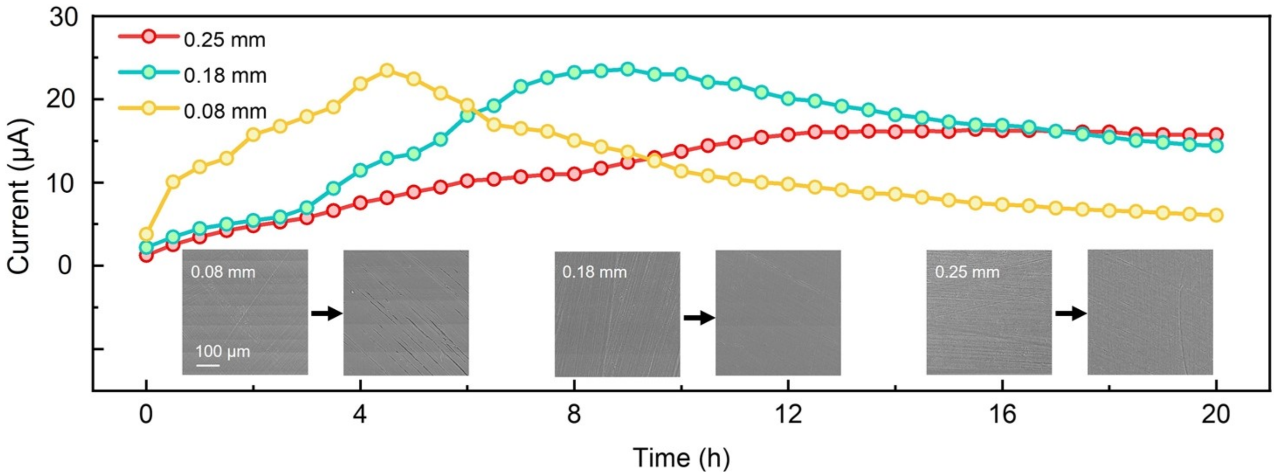

Fig. S6 Durability test of conventional TENG with different thickness PTFE. Insets are the SEM of PTFE before and after friction.

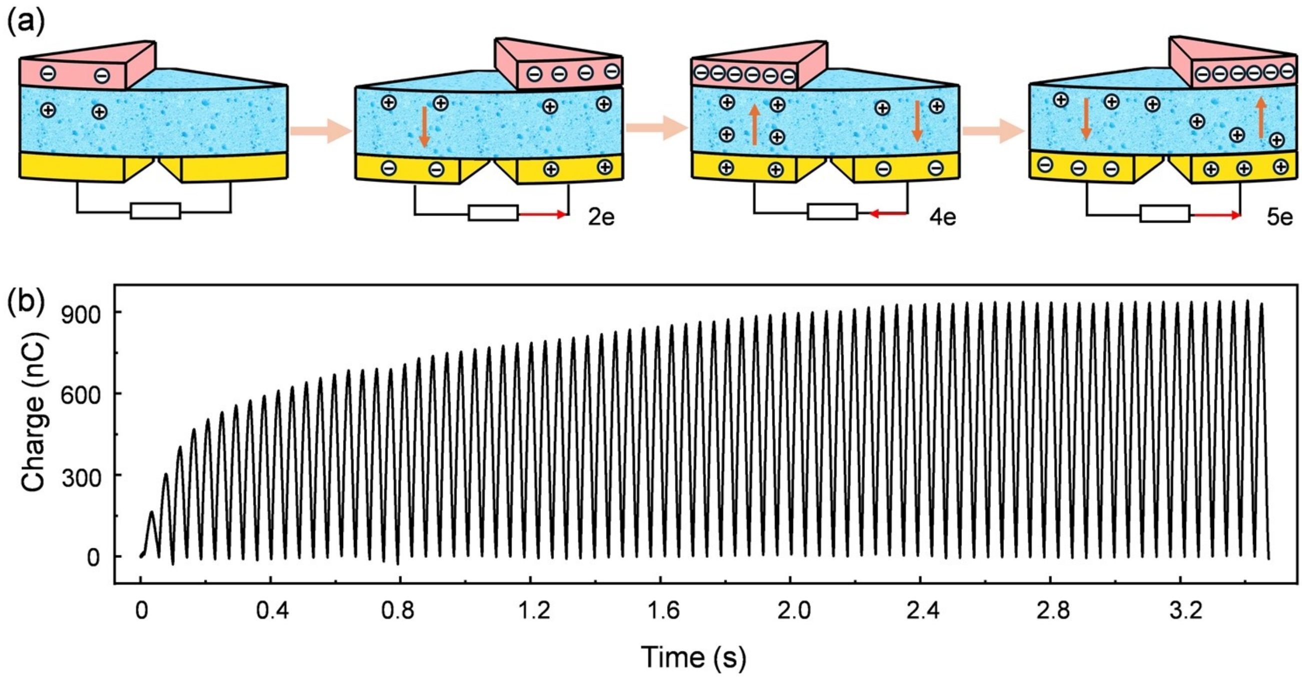

Fig. S7 a)-b) Schematic diagram of triboelectric electrification process and corresponding charge waveform of CM-TENG.

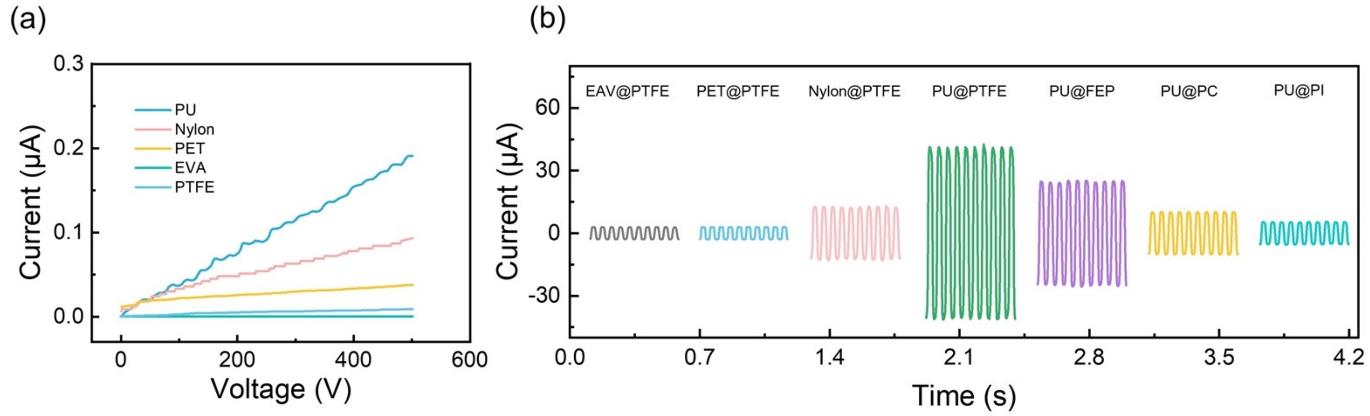

Fig. S8 a)-b) I-V curves of materials and current output of CM-TENG with different material combinations.

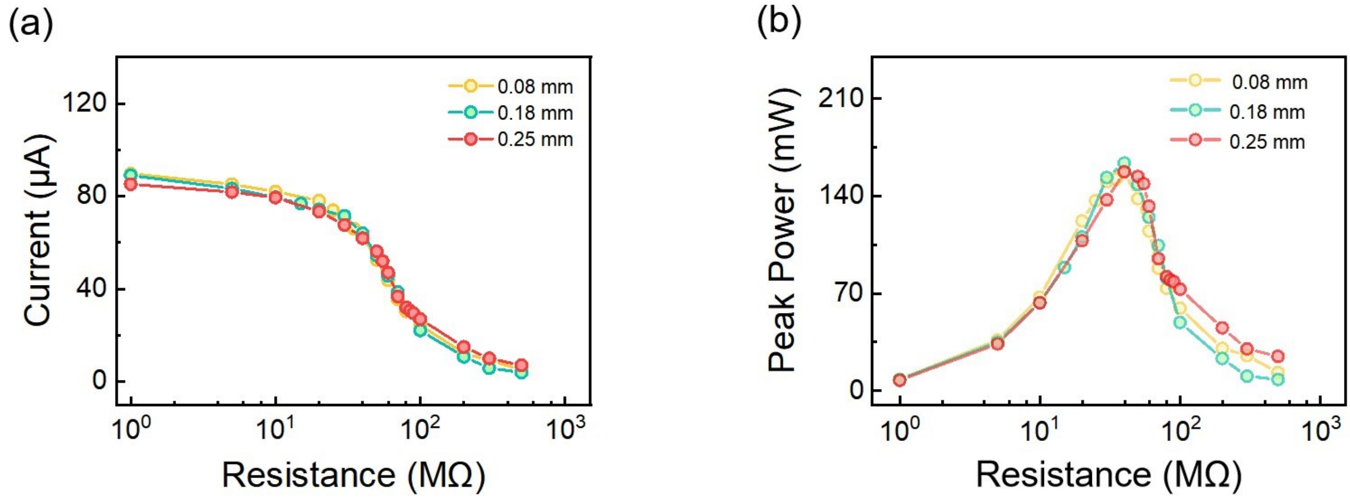

Fig. S9 Effect of CM-TENG's a) output current and b) matching impedance on PTFE thickness.

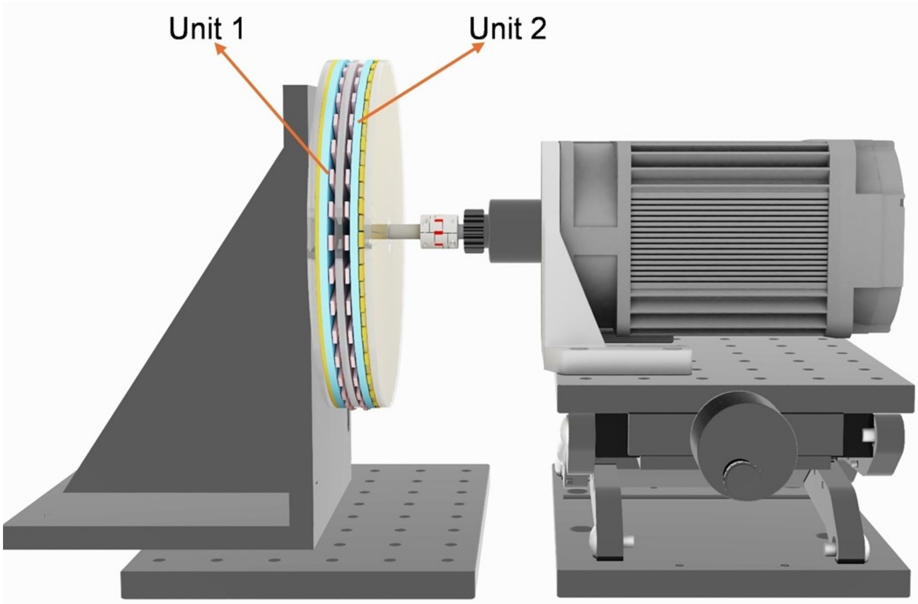

Fig. S10 Schematic diagram of testing setup.

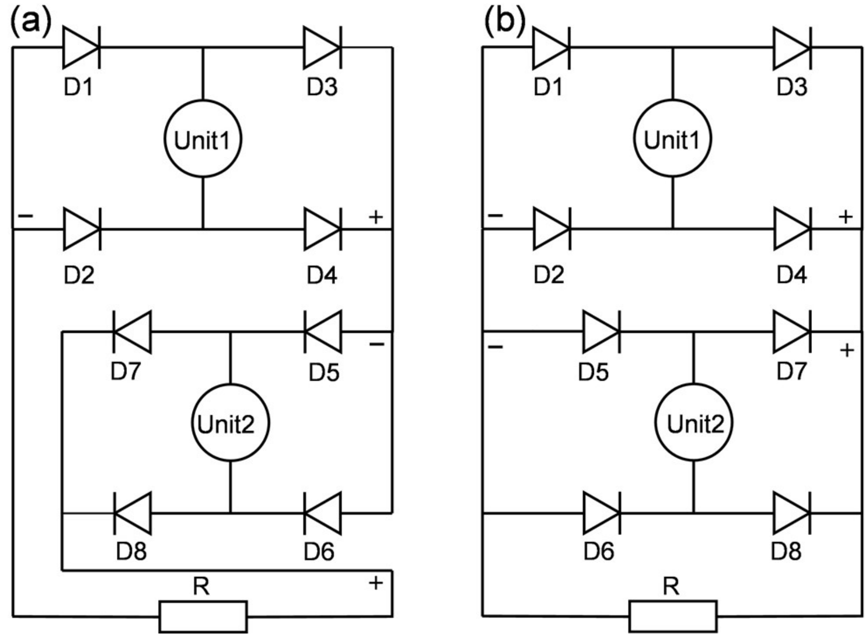

Fig. S11 a)-b) Circuit diagram of series and parallel connection of Unit 1 and Unit 2.

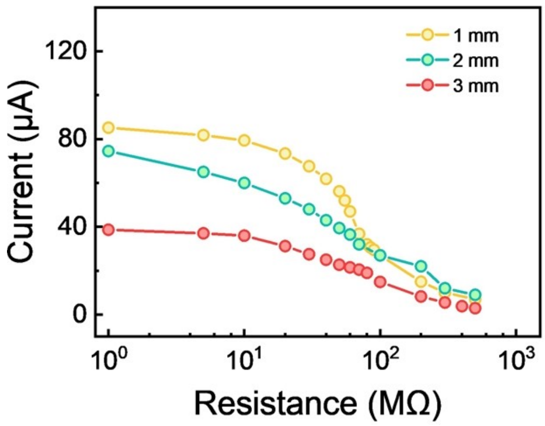

Fig. S12 Relationship of CM-TENG’s output current on PU thickness.

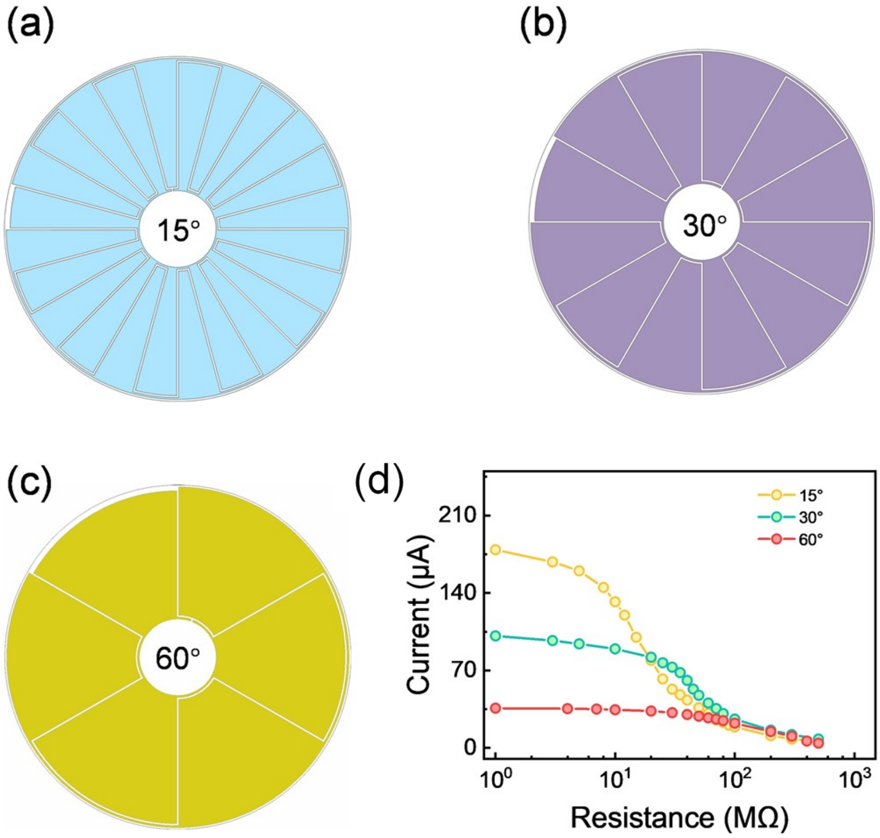

Fig. S13 a)-c) Schematic diagram of different electrode degrees. d) Effect of CM-TENG's output current on different electrode degree.

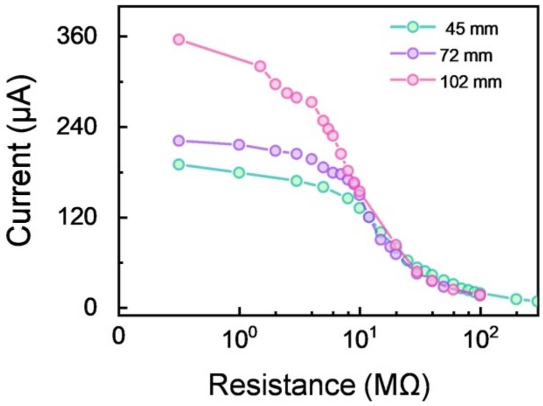

Fig. S14 Dependence of CM-TENG's output current on electrode radius.

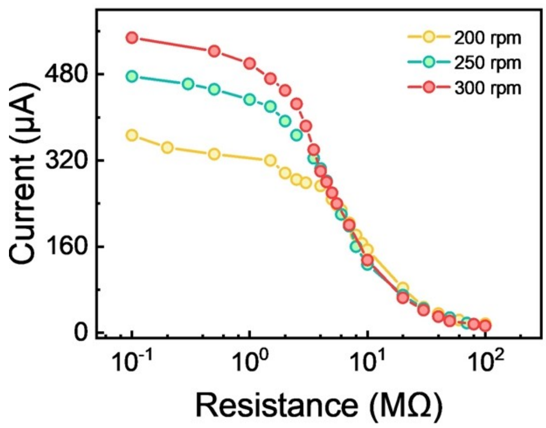

Fig. S15 Effect of CM-TENG's output current on rotation speed.

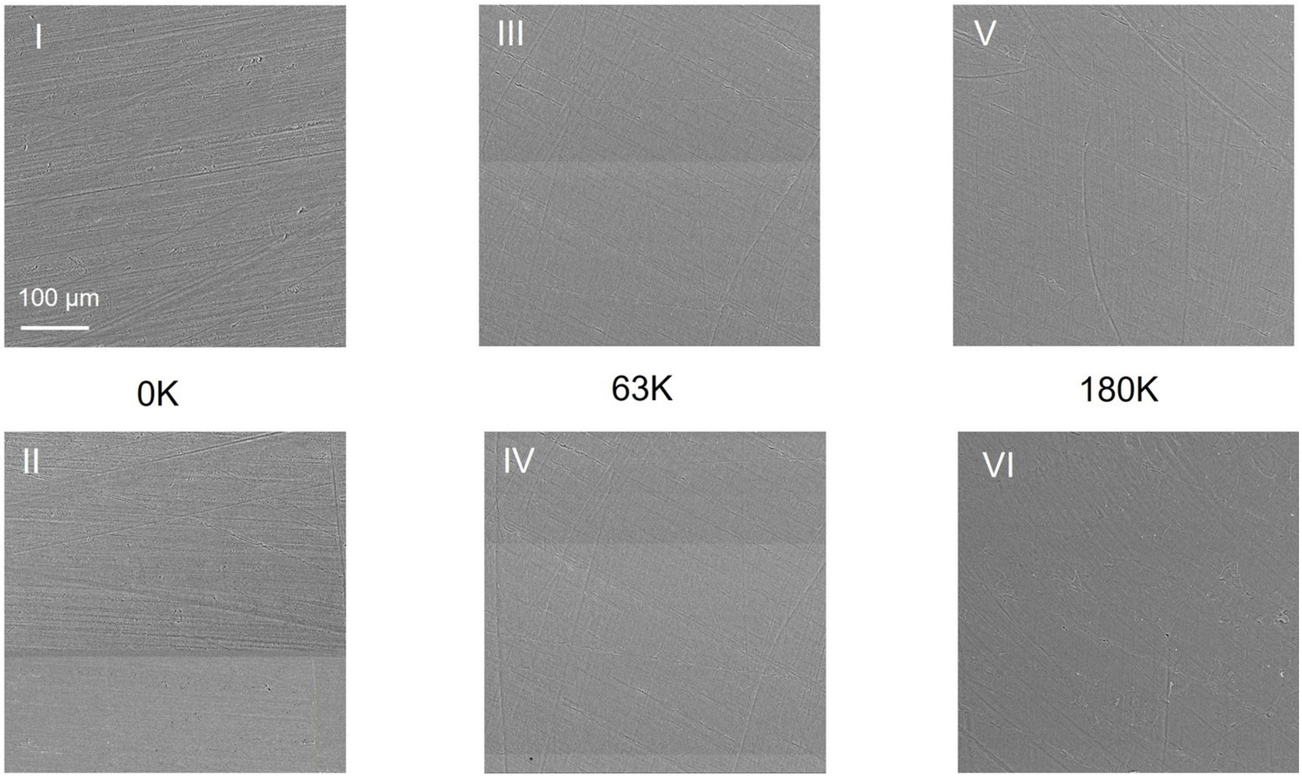

Fig. S16 PTFE’s SEM of Unit 1 at 0K, 63K, and 180K working cycles (I-III-V). PTFE’s SEM of Unit 2 at 0K, 63K, and 180K working cycles (II-VI-VI).

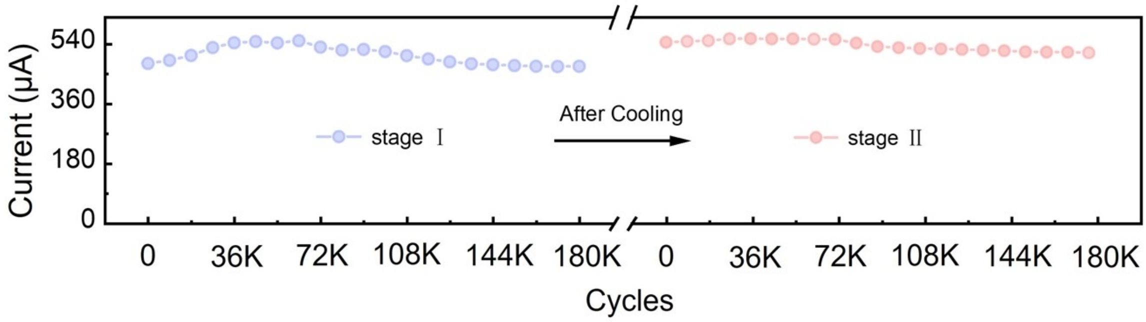

Fig. S17 Output current for CM-TENG to restart after cooling.

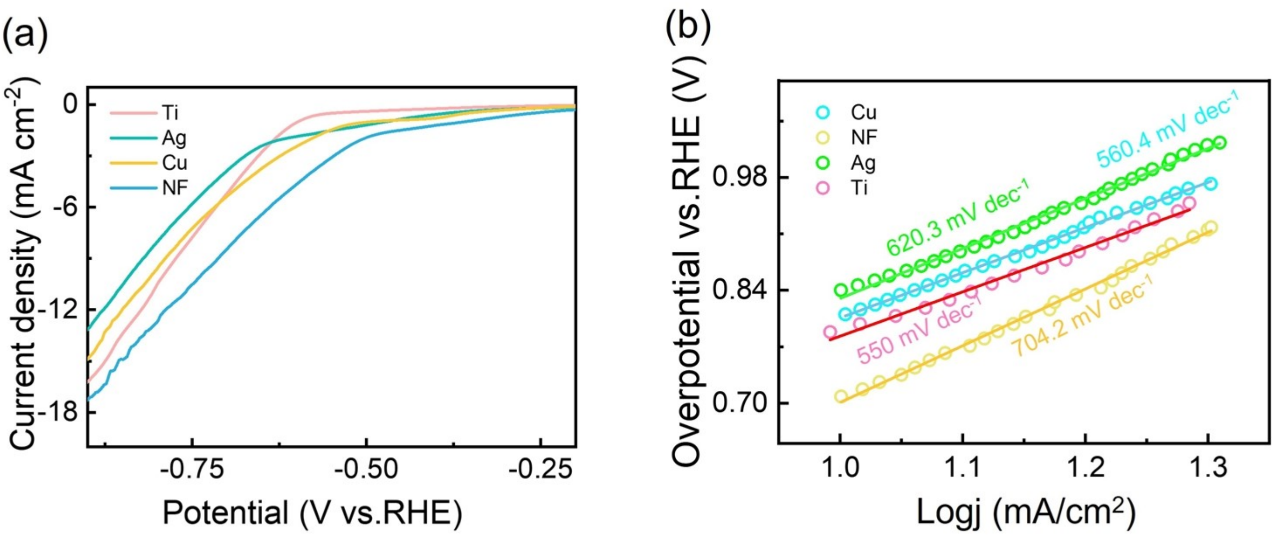

Fig. S18 a)-b) LSV curve and Tafel slope of the HER with different electrodes in 1.0 M KOH.

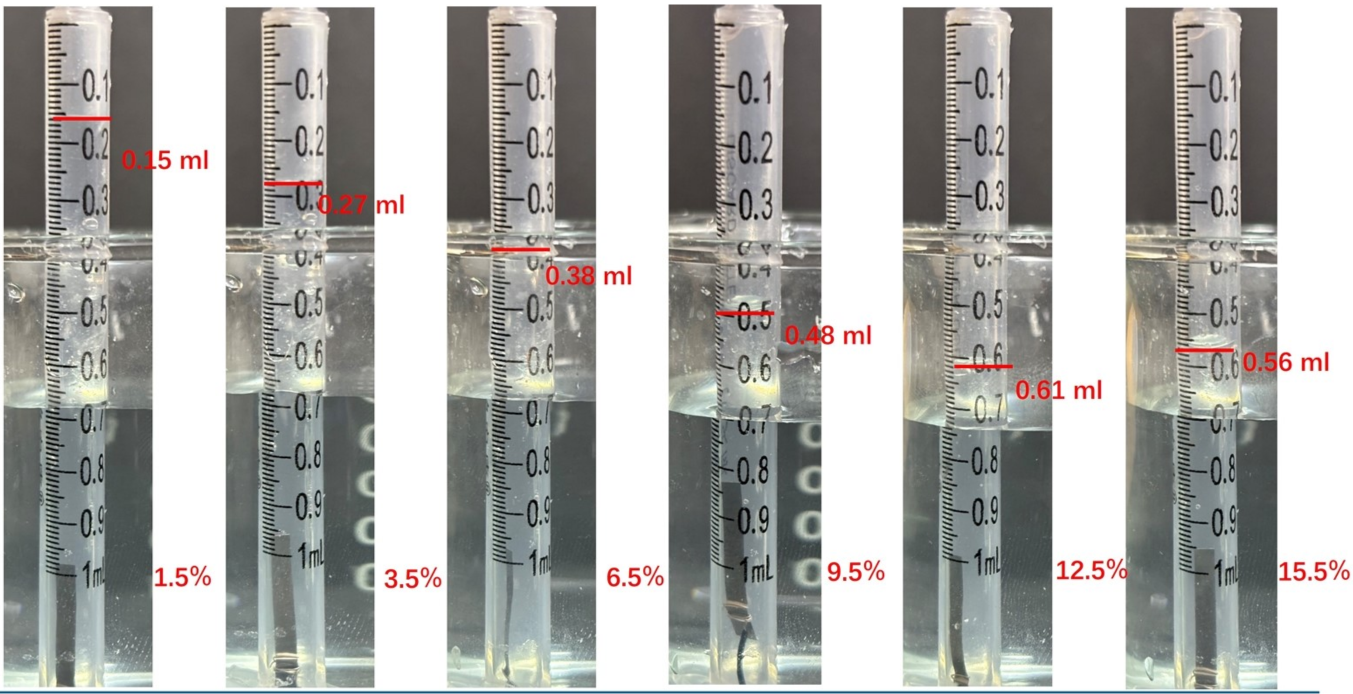

Fig. S19 Dependence of Ti@Pt's hydrogen production rate on the concentrations of saline water at a current density of 10 mA cm^{-2} and 12 minutes.

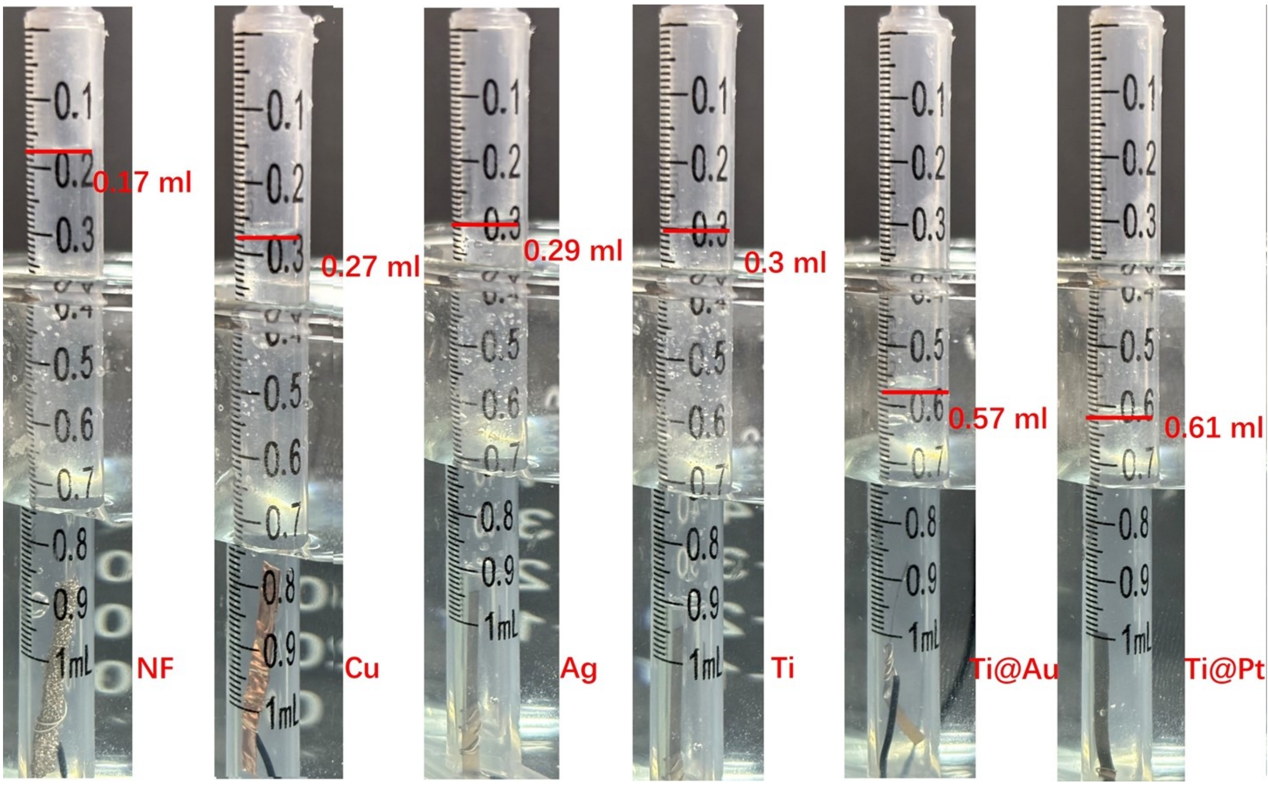

Fig. S20 Physical photographs of hydrogen production for different electrode materials in 12.5 wt% saline solution.

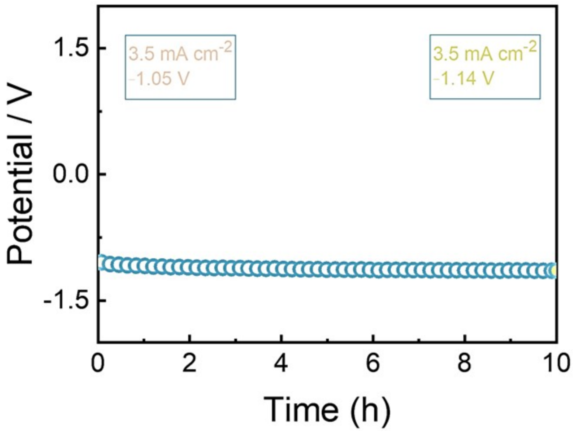

Fig. S21 Chronopotentiometry testing of Ti@Pt in simulated seawater with 12.5 wt% salinity at a constant current density of 3.5 mA cm^{-2} for 10 hours.

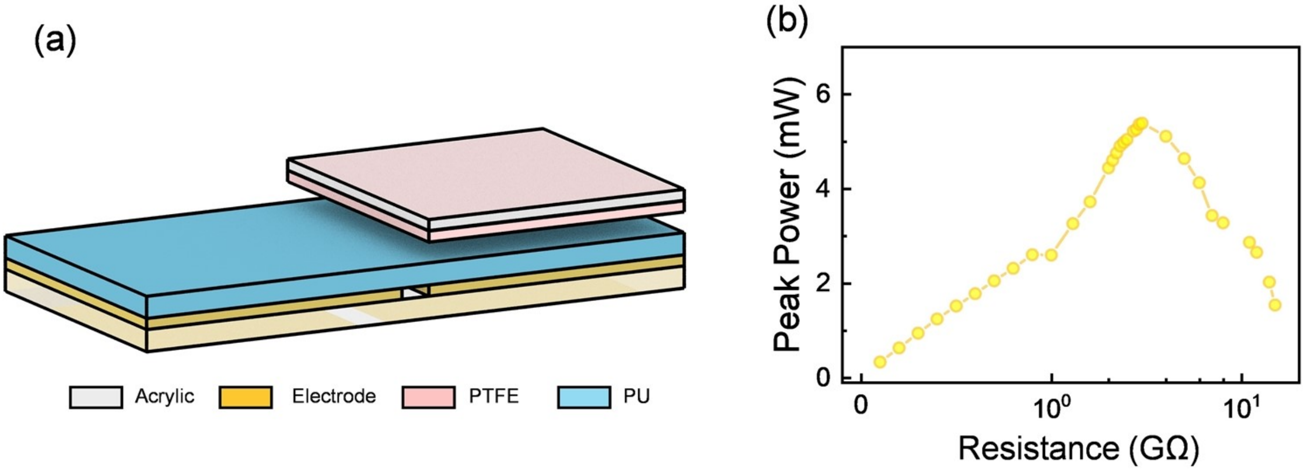

Fig. S22 a)-b) Structure diagram of sliding CM-TENG and the peak power under different external resistances.

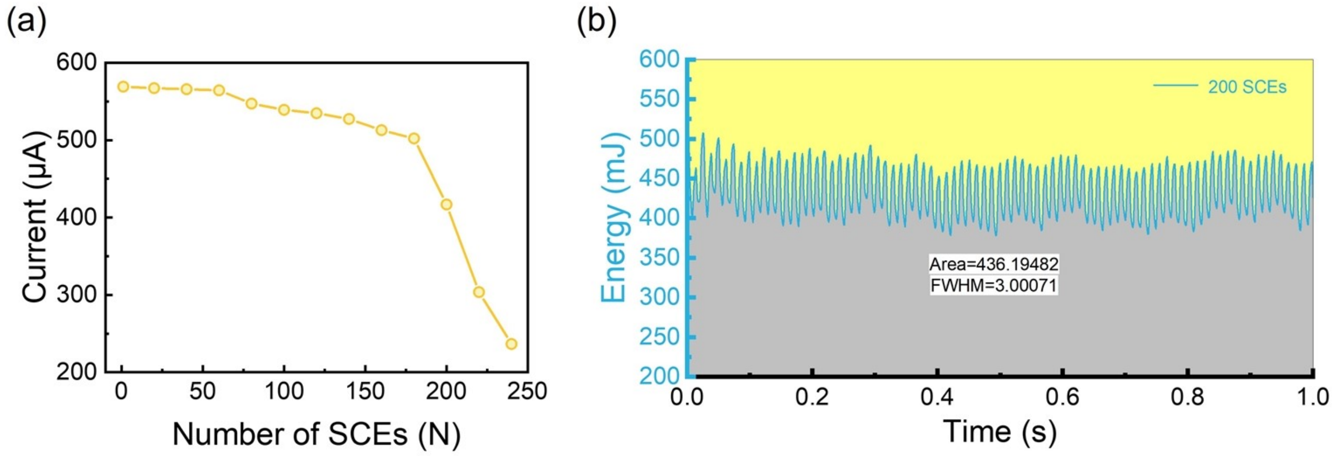

F

ig. S23 a) Dependence of CM-TENG's output current on number of SCEs. b) Output energy per unit time of CM-TENG when connected with 200 SCEs.

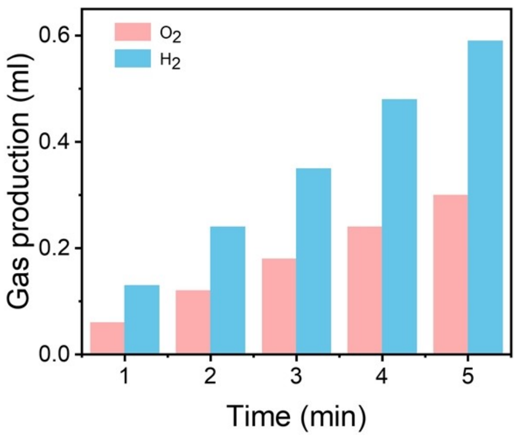

Fig. S24 Generation of O_2 and H_2 per minute

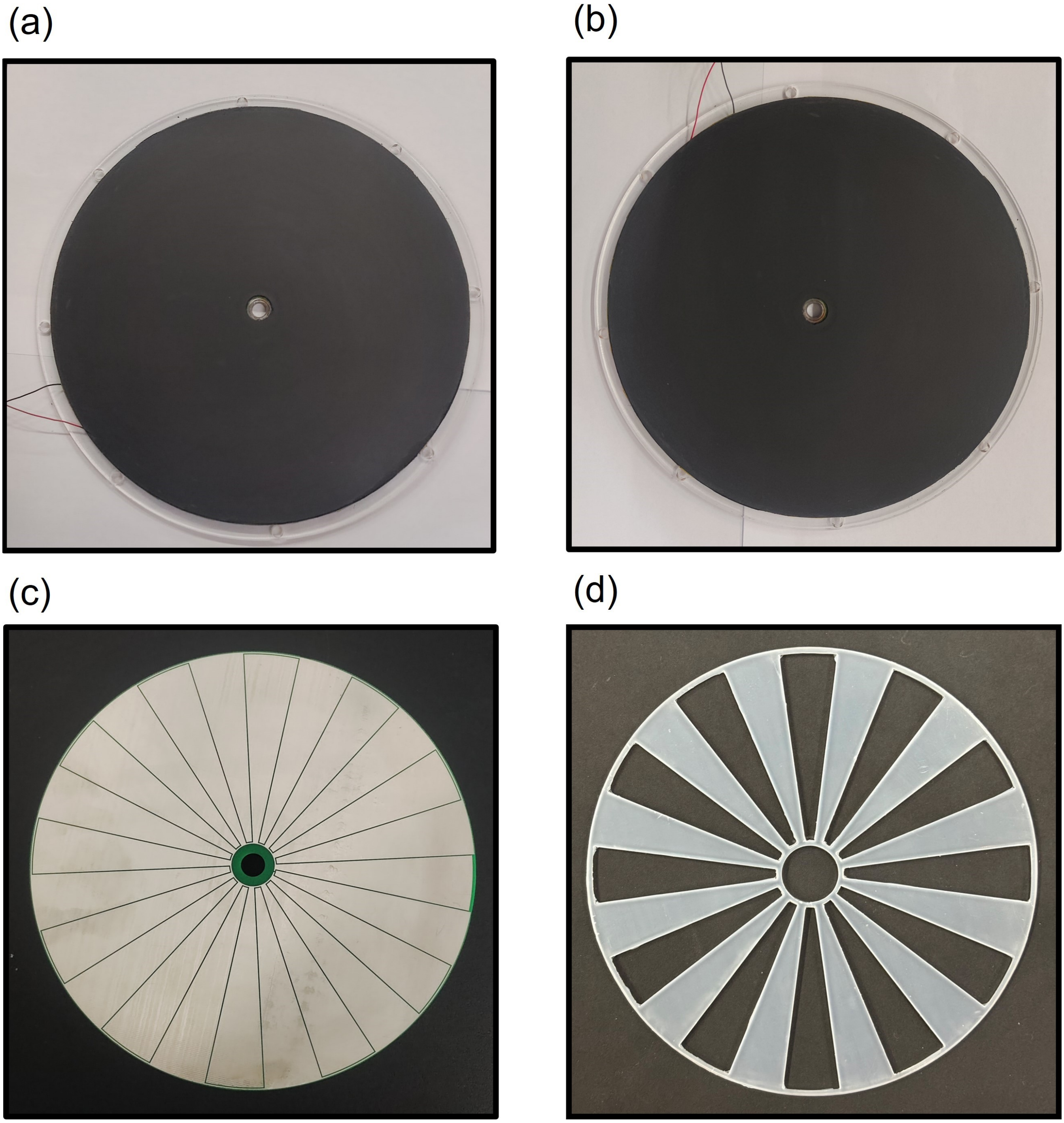

Fig. S25 a)-d) Physical photographs of Unit 1's stator, and Unit 2's stator, the deposited grid-shaped copper electrodes, and the rotor.

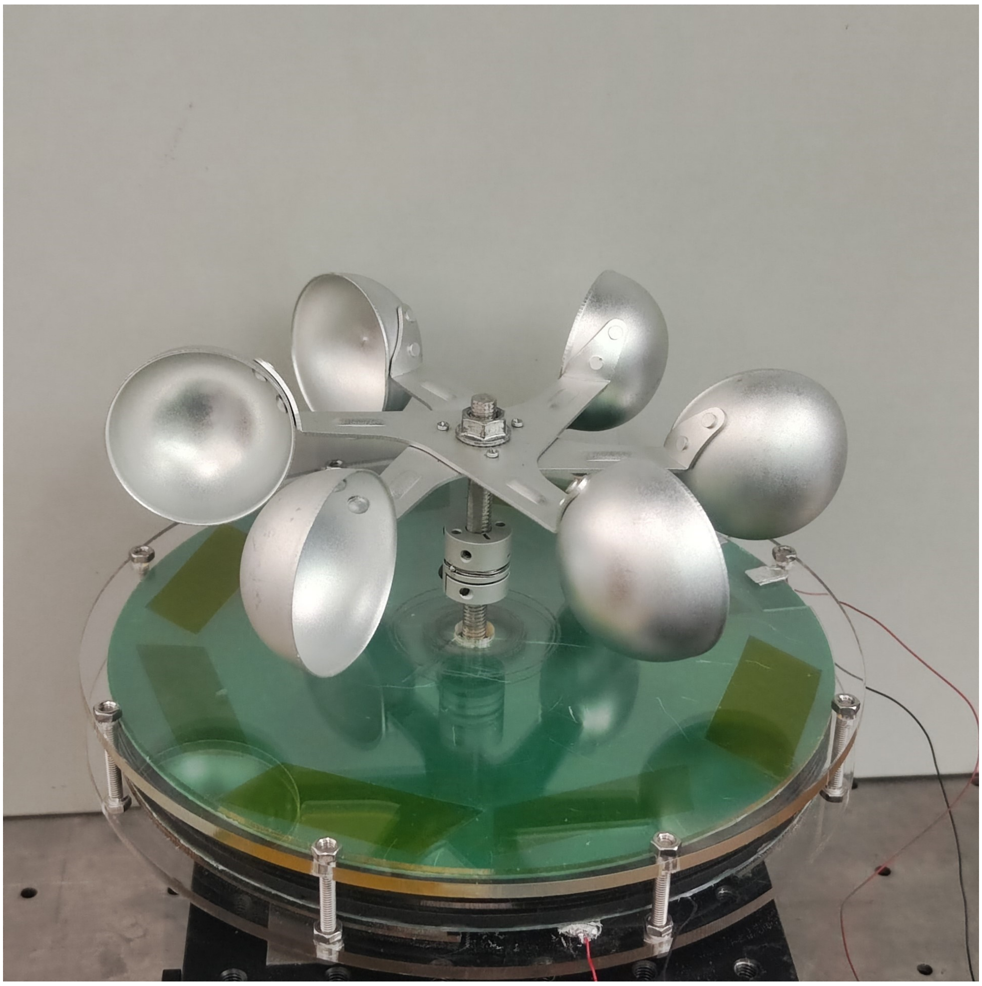

Fig. S26 Physical photograph of CM-TENG' overall structure.